Analysis of ultraviolet P Cygni profiles in the spectra of O-type stars

F. Nemry[1] and J. Surdej[2]
Institut d'Astrophysique de Liège
avenue de Cointe, 5
B-4000 Liège
Belgium

Abstract

In the framework of the analysis and interpretation of observed P Cygni line profiles, we describe and compare the nth order moment method with the line profile fitting technique. We then point out that, if we want to make a proper statistical study of the UV P Cygni profiles observed in the spectra of O-type stars, we have to take into account the severe pollution effects due to a forest of FeIV and FeV absorption lines. We discuss a method allowing to correct the observed profiles for the presence of photospheric lines and we give estimates of the error on $\dot{M}$ caused by this pollution.

Keywords : Lines: formation, Lines: identification, Lines: profile, Spectroscopy, Stars: mass loss.

1 The nth order moments W_n method

1.1 Definition

The first order moment W_1 of a P Cygni line profile was first introduced by Castor et al. (1981) in the framework of the Sobolev approximation. It was generalized by Surdej (1982, 1983a, 1983b, 1985), Surdej and Hutsemékers (1990) and Hutsemékers and Surdej (1990).

The nth order moment of a resonance P Cygni line profile formed in an expanding envelope with a terminal velocity v_∞ is defined by

$$W_n = \left(\frac{c}{\lambda_{12} v_\infty}\right)^{n+1} \int_{line} \frac{E(\lambda) - E_c(\lambda)}{E_c(\lambda)} (\lambda - \lambda_{12})^n d\lambda, \tag{1}$$

where $\frac{E(\lambda)}{E_c(\lambda)}$ is the normalized line profile function and λ_{12} is the rest wavelength of the line profile in the frame of the observer.

If we pose

$$X = -\frac{\nu - \nu_{12}}{\nu_{max} - \nu_{12}}, \tag{2}$$

we find that

$$W_n = \int_{-1}^{+1} \frac{E(X) - E_c(X)}{E_c(X)} X^n dX. \tag{3}$$

[1] Aspirant au Fonds National de la Recherche Scientifique (Belgium)
[2] Chercheur Qualifié au Fonds National de la Recherche Scientifique (Belgium)

From this definition, we see that W_0 is the equivalent width. For n odd, W_n does only depend on the opacity structure and for n even, W_n depends on both the opacity and velocity structures.

1.2 Physical meaning of the moments

1.2.1 The first order moment

a) Optically thin lines : Making use of the fact that the fictitious opacity at a given point in the envelope is

$$\tau_{12}^r(X') = \dot{M} f(X'),$$

where X' is the reduced velocity $\frac{v(r)}{v_\infty}$, $\dot{M}$ is the mass loss rate and $f(X')$ is a function depending on the ionization and the velocity structures, it can be shown that, for the case of optically thin lines, the moment W_1^0 is given by

$$W_1^0 = \dot{M}\langle n_1 \rangle \frac{q_c K_{12}}{v_\infty^2}, \tag{4}$$

which implies that W_1^0 is directly proportional to $\dot{M}$ irrespectively of the opacity and velocity structures, turbulence, rotation, or relativistic effects. Similar relations may also be derived for the case of resonance doublets or subordinate lines. The opacity law may be then conveniently re-written in the form

$$\tau_{12}^r = W_1^0 \frac{n_1(X')}{q_c \langle n_1 \rangle} \frac{1}{L^2 X'} \frac{dL}{dX'}. \tag{5}$$

In the above expressions, q_c and K_{12} are two constants, $\langle n_1 \rangle$ represents the mean ionization fraction across the envelope and L is the radial distance expressed in terms of the stellar radius.

b) Optically thick lines : W_1 is no longer proportional to $\dot{M}$, but by means of Eqs. (4) and (5), it is possible to compute W_1 as a function of W_1^0 and to construct curves of astrophysical interest.

1.2.2 The other moments

Making a same development for the other moments W_n as for W_1, we may show that W_2^0 and W_3^0 are related to the momentum and the kinetic energy rate of the envelope, respectively.

1.3 "log W_n - log W_n^0" and "log W_n - log $W_{n'}$" diagrams

Fig. 1 illustrates, for $n = 2$, the "$\log W_n - \log W_n^0$" diagram constructed for 18 models based on relations listed in table 1. Given a measured moment W_n, it is possible to derive W_n^0 by just locating it in the diagram. In this diagram, we see that for unsaturated lines W_n is on the linear part of the curve which implies that W_n^0 is independent of the model. For saturated lines, the derived value for W_n^0 becomes very sensitive to the adopted model.

Figure 1: The "$\log W_2 - \log W_2^0$" diagram computed for 3 velocity fields and 6 opacity laws (see table 1) under the Sobolev approximation.

(A)	$X' = -X_{min} + (1 + X_{min})(1 - 1/\sqrt{L})$
(B)	$X' = -X_{min} + (1 + X_{min})(1 - 1/L)$
(C)	$X' = \sqrt{1 - (1 - X_{min}^2)/L}$
(α)	$\tau_{12}^r \propto (L^2 X' dX'/dL)^{-1}$
(β)	$\tau_{12}^r \propto 1 - X'$
(γ)	$\tau_{12}^r \propto 1$
(δ)	$\tau_{12}^r \propto \sqrt{1 - X'}$
(ϵ)	$\tau_{12}^r \propto (1 - X')^2$
(η)	$\tau_{12}^r \propto 1/X'$

Table 1. The 3 velocity fields and 6 opacity laws used as representative to describe the properties of expanding envelopes.

Similar diagrams are easily constructed for W_0, W_1, and W_3.
Furthermore, "$\log W_n - \log W_{n'}$" diagrams may also be used in order to estimate the velocity and opacity structures.

In conclusion, we can say that the nth order moment method is well adapted to the study of properties of expanding envelopes in which P Cygni profiles are formed.

1.4 Comparison with the line profile fitting technique

1) The line profile fitting technique and the moment method are complementary : having made use of the latter one to determine W_n^0 and the velocity and opacity laws, the fitting method should be an interesting tool to confirm and/or refine the previous results.

2) Measured moments are insensitive to the spectral resolution (Castor, 1981). The nth order moments method is then also well adapted to the study of under-resolved P Cygni

line profiles.

3) The nth order moment method allows one to consider simultaneously large samples of data's via the construction of observational "$\log W_n - \log W_{n'}$" diagrams. Comparison of these diagrams with theoretical ones is very straightforward.

4) Contrary to the line fitting method where it is difficult to derive uncertainty for calculated parameters like τ_{12}^r, X', W_1^0, realistic error estimates of the derived parameters W_n^0 can be easily assigned on the basis of "$\log W_n - \log W_n^0$" diagrams. Indeed, from the observed dispersion of the "$\log W_n - \log W_n^0$" curves, we can easily estimate the upper value W_n^U such that, due to the uncertainty in the choice of the model, the error on W_n^0 is less than 100% : $W_0^U = 0.31$, $W_1^U = 0.24$, $W_2^U = 0.17$, $W_3^U = 0.15$.

5) None of the two methods can be applied to the case of saturated profiles (see the asymptotic behaviour of the curves in Fig. 1 for large values of W_n^0).

6) Except for the case where lines of the same elements are observed, none of the above methods solves the ultimate problem of determining the fractional ionization abundances.

1.5 Effects of turbulence

In many cases, profiles computed under the Sobolev approximation cannot match the observed profiles : it is necessary to include the presence of turbulence in the envelope when solving the radiative transfer equation (cf. Lamers et al., 1987).

For optically thin lines, it can be shown that the profile formed in a turbulent envelope is simply the convolution by the absorption profile of the P Cygni one which would be formed in the same envelope without turbulence. This leads to simple relations between the corresponding moments W_n and W_n^s, respectively (Surdej, 1985). For instance,

$$W_0 = \frac{W_0^s}{(1 + \frac{\bar{u}}{v_\infty})},$$

$$W_1 = \frac{W_1^s}{(1 + \frac{\bar{u}}{v_\infty})^2}.$$

Adequate combinations of the moments should allow us to estimate both W_n^0 and $\frac{\bar{u}}{v_\infty}$.

2 Pollution of P Cygni line profiles by FeIV and FeV photospheric lines in the ultraviolet spectrum of O-type stars

2.1 Identification of the photospheric lines

The atlas of IUE O-type stars published by Walborn, Nichols-Bohlin and Panek (1985) provides us with a unique tool to study the mass loss phenomena taking place in the atmospheres of early-type stars. Trying to measure the moments of the resonance line transitions due to CIV, SiIV, HeII and NIV, we encountered serious difficulties when setting the level of the local continuum which is severely affected by a forest of FeIV and FeV photospheric lines. This prevents one from making any accurate measurements (see Figs. 3 and 4).

Figure 2: The "$\log W_1 - \log W_1^0$" curves obtained with the model $B.\beta$ of table 1 and for different turbulent velocities : $\frac{\bar{u}}{v_\infty} = 0(\square), 0.1(+), 0.2(\diamond), 0.3(\triangle)$

Figure 3: (a) A representative SiIV P Cygni line profile for supergiant O-type stars as constructed from the average spectrum of 28 objects selected in the WNP atlas. The vertical lines at the top and at the bottom of this figure represent the expected positions and strengths of FeV and FeIV lines, respectively. (b) same as (a) but for a sub-sample of 20 main-sequence and dwarf O-type stars.

Figure 4: Same as Fig. 3 but for the CIV P Cygni line profiles as constructed from the average spectrum of the 50 first (upper line) and the 48 last (lower line) O-type stars in the WNP atlas.

2.2 What are the effects due to the presence of iron lines?

2.2.1 A correcting method

In view of the obvious effects of the FeIV and FeV lines on the shape of the P Cygni UV line profiles (Figs. 3 and 4), one has to estimate the error introduced by the presence of the former on the derived mass loss rates. In the framework of the Sobolev approximation, we have established a method for "depolluting" the observed P Cygni profiles and restoring the profile that would have been recorded in the absence of photospheric lines.

We showed that (Nemry, Surdej, Hernaiz, 1990), for negative frequencies X in the profile :

$$E(X) \simeq \frac{E^p(X)}{E_c(X)}, \tag{6}$$

and that for positive frequencies X,

$$E(X) \simeq \frac{E^p(X) - E_c(X)}{\langle E_c \rangle_{X \leq 0}} + 1, \tag{7}$$

where $E^p(X)$ is the observed flux profile, $E_c(X)$ the continuum flux, $E(X)$ the corrected flux profile and $\langle E_c \rangle_{X \leq 0}$ is the mean continuum flux over the negative frequencies covering the profile.

This method was tested for different values of W_1^0 and for non turbulent or turbulent atmospheres (see Fig. 5). In view of the excellent results illustrated in figures 5a and 5b, the use of our correcting method is plainly justified.

2.2.2 Correction of profiles and estimates of the error on $\dot{M}$

In view of the results in Fig. 6 and table 2, it is not sufficient to set a pseudo-continuum to correct for the effects of underlying photospheric lines. Let us notice that in some cases, the error on the estimate of $\dot{M}$ may exceed 100%.

Figure 5: (a) The dashed line curve illustrates the average continuum in the spectral range of the CIV doublet resonance line for 5 stars showing no wind effects. This continuum was used in order to simulate a "polluted" resonance P Cygni line profile (solid line). With Eqs. (6) and (7), we corrected this "polluted" profile and obtained the dotted line curve. The crosses indicate the corresponding P Cygni profile calculated with a flat continuum. The turbulent velocity was null. (b) same as (a) but for $\frac{\bar{u}}{v_\infty} = 0.1$.

Figure 6: (a) The solid line in this figure displays the original SiIV P Cygni line profile of supergiant O-type stars as illustrated in Fig. 3a. The dashed line corresponds to the former line profile corrected for the photospheric absorption lines by means of the stellar spectrum in Fig. 3b, unaffected by stellar wind effects. The horizontal lines labelled A, B, C represent different settings of the local stellar continuum used when measuring the first order moment W_1 (see text). (b) same as (a) but for the representative CIV P Cygni line profile constructed from a sample of 20 main-sequence and dwarf O-type stars.

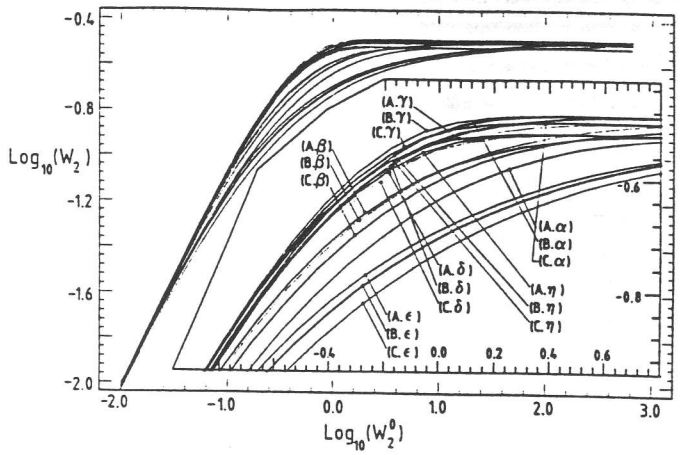
Log10(W2)
Log10(W20)
(A.γ)
(B.γ)
(C.γ)
(A.β)
(B.β)
(C.β)
(A.α)
(B.α)
(C.α)
(A.δ)
(B.δ)
(C.δ)
(A.η)
(B.η)
(C.η)
(A.ε)
(B.ε)
(C.ε)

Fig 1

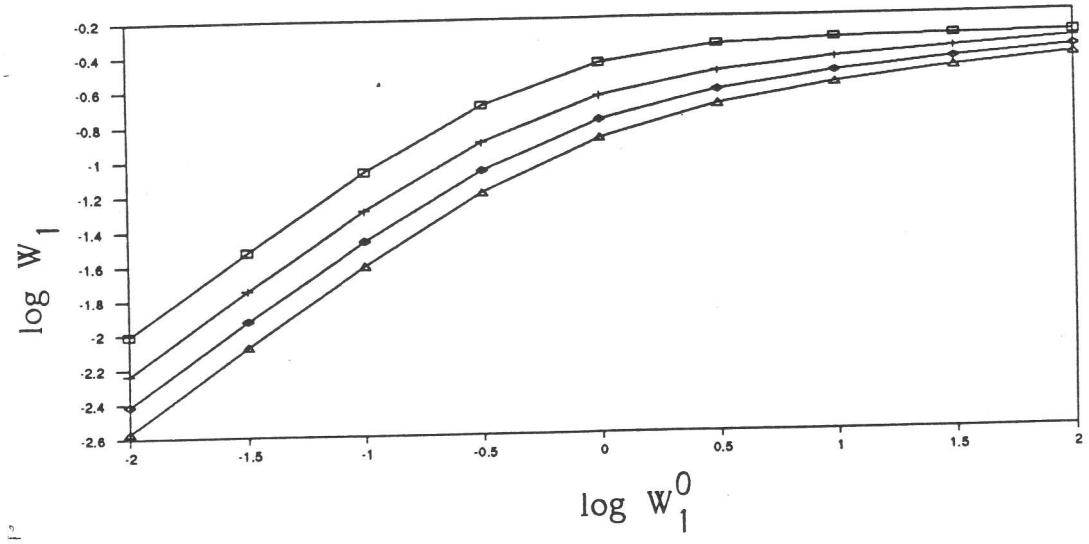
log W1
log W10

Fig 2

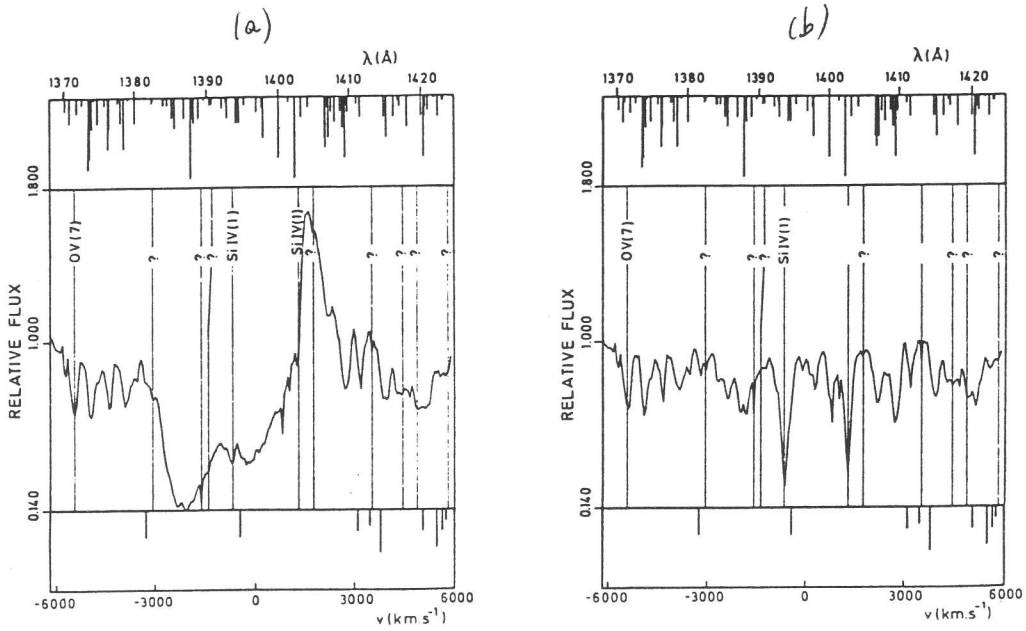
(a)
(b)
λ(Å)
RELATIVE FLUX
OV(7)
Si IV(1)
v (km.s-1)

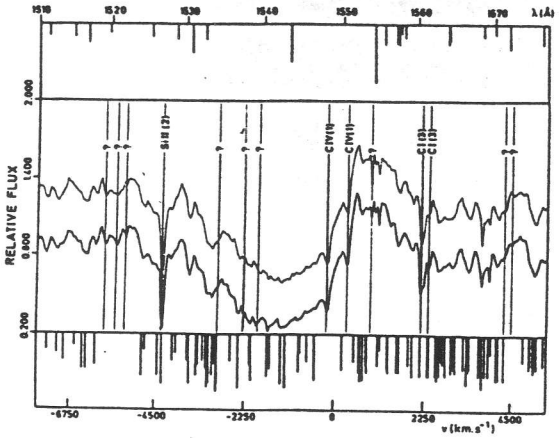
RELATIVE FLUX
v (km.s⁻¹)

Fig 4

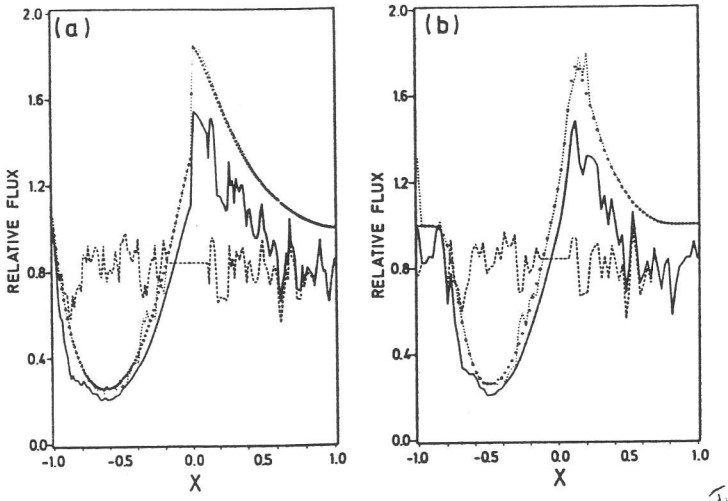
(a)
(b)
RELATIVE FLUX
X

Fig 5

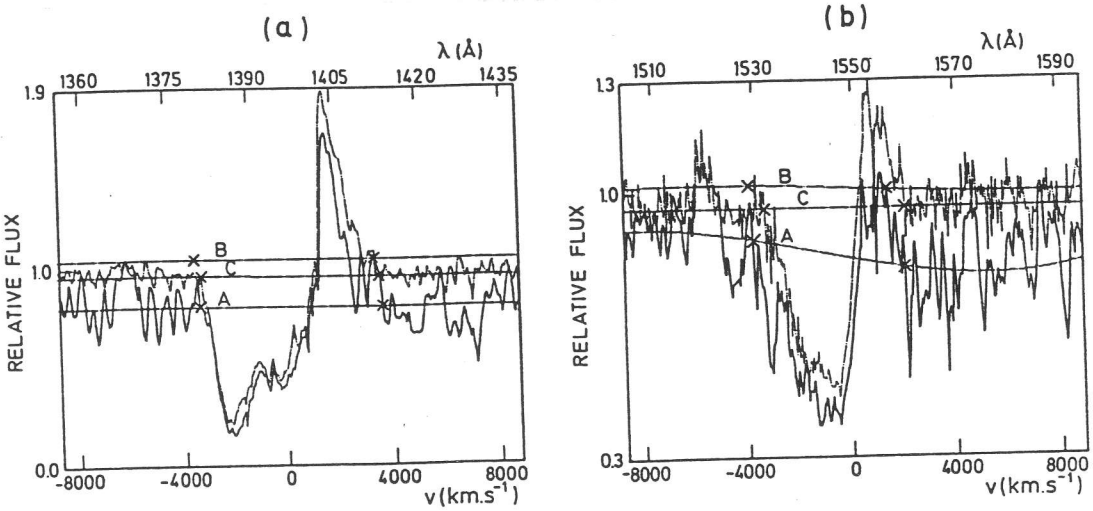
(a)
(b)
λ(Å)
RELATIVE FLUX
A
B
C
v(km.s⁻¹)